

www.acsanm.org Article

High-Performance Strain Sensors Based on Vertically Aligned Piezoelectric Zinc Oxide Nanowire Array/Graphene Nanohybrids

Mohan Panth,* Brent Cook, Young Zhang, Dan Ewing, Ashely Tramble, Amy Wilson, and Judy Wu*



Cite This: ACS Appl. Nano Mater. 2020, 3, 6711–6718



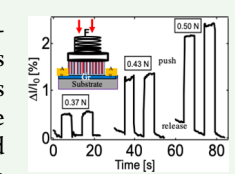
ACCESS

Metrics & More

Article Recommendations

Supporting Information

ABSTRACT: A nanohybrid piezoelectric strain sensor was fabricated by growing vertically aligned (0001)-oriented crystalline zinc oxide nanowires directly on graphene (ZnO-VANWs/Gr) using a facile seedless hydrothermal process. Under mechanical strains, the induced piezoelectric effect on the ZnO-VANWs transduces to a piezoelectric gating effect at the ZnO-VANWs/Gr interface, resulting in a modulation of the conductivity of the Gr channel through electrostatic doping. The vertical alignment of the (0001)-oriented ZnO-VANWs on Gr is ideal to achieving high strain sensitivity, and a low-defect ZnO-VANWs/Gr interface obtained in the seedless hydrothermal process is key to realizing high sensitivity and fast response. Indeed, a



high sensitivity up to $3.15 \times 10^{-2} \, \mathrm{kPa^{-1}}$ was obtained on the ZnO-VANWs/Gr strain sensors at lower pressures of $1.1 \times 10^{-6} - 11$ Torr, together with a fast response time of $\sim 0.10 \, \mathrm{s.}$ In particular, these results represent enhancement factors of ~ 7 and 8, respectively, as compared to strain sensors of a similar structure, except having a polycrystalline ZnO seed layer on Gr for the growth of ZnO-VANWs. Therefore, our result illustrates the critical importance of the low-defect interface of the ZnO-VANWs with Gr formed in the seedless ZnO-VANW growth for realizing an optimal electrostatic gating of Gr. In addition, the ZnO-VANWs/Gr nanohybrids can be readily scaled up using the seedless hydrothermal process for commercial applications in optoelectronics and sensors.

KEYWORDS: piezoelectric gating, graphene, zinc oxide nanowires, strain sensor, hydrothermal growth, nanohybrid

1. INTRODUCTION

High-performance strain sensors are desired for a large spectrum of emerging applications in wearable electronics, robotics, health care, and infrastructure monitoring. Among others, piezoelectric/graphene nanohybrids are of particular interests to transduce a mechanical deformation from the piezoelectric component to the piezoelectric gating on graphene (Gr), taking the advantages of Gr's high mechanical strength,⁷ flexibility, and high carrier mobility.⁸ The piezoelectric nanohybrid strain sensors can be further divided into two main types: (1) piezoresistive^{9,10} and (2) piezoelectric gating 11,12 based on different sensing mechanisms. Piezoresistive strain sensors rely on resistance changes of piezoresistive materials under applied pressure/strain. Extensive progress has been made in piezoresistive sensors primarily based on composites of nanostructures of zinc oxide (ZnO), lead zirconate titanate (PZT), lead titanate (PbTiO₃), etc, ^{13–15} mixed with polymers including poly(vinylidene fluoride) (PVDF), polydimethylsiloxane (PDMS), and poly(methyl methacrylate) (PMMA).^{16–18} After the discovery of Gr,¹⁹ its derivatives have also been used as filler materials into the composites to enhance the conductivity and thereby sensitivity and stretch ability. 9,20,21 A highly stretchable and sensitive strain sensor fabricated by Tang et al. based on reduced graphene oxide/elastomer (rGO/PDMS) shows a sensitivity as high as 630 of gauge factor under 21.3% applied strain, which is an order of magnitude enhancement as compared to the counterparts without rGO. This improvement is attributed to

the enhanced change in contact resistance among rGO sheets during their mechanical deformation. Similarly, a sensitivity of $9.4 \times 10^{-3}~\mathrm{kPa^{-1}}$ under pressures of $0-1400~\mathrm{Pa}$ and response times of $5-7~\mathrm{ms}$ were obtained for the PbTiO₃ NWs/Gr-based piezoresistive sensor. While these piezoresistive devices have a simple device structure and low fabrication cost, they require a high power to operate and hence, further improvement is necessary for them to be suitable for low-power or self-power applications.

In contrast to the case of the piezoresistive devices that rely on the volume effect of the sensor, piezoelectric-gating devices based on the interface effect of the strain-induced piezoelectric surface charges may provide a promising scheme for strain sensors that could be operated at a low power. In particular, nanohybrids that combine the piezoelectric nanostructures and Gr allow a unique design of the piezoelectric-gating sensors. For example, Sun et al. The made a piezoelectric potential powered coplanar gated Gr field effect transistor (GFET) where ion gel was photopatterned on the channel of Gr fabricated using chemical vapor deposition (CVD) and a part of Gr gate electrodes for effective piezoelectric potential

Received: April 28, 2020 Accepted: July 2, 2020 Published: July 2, 2020





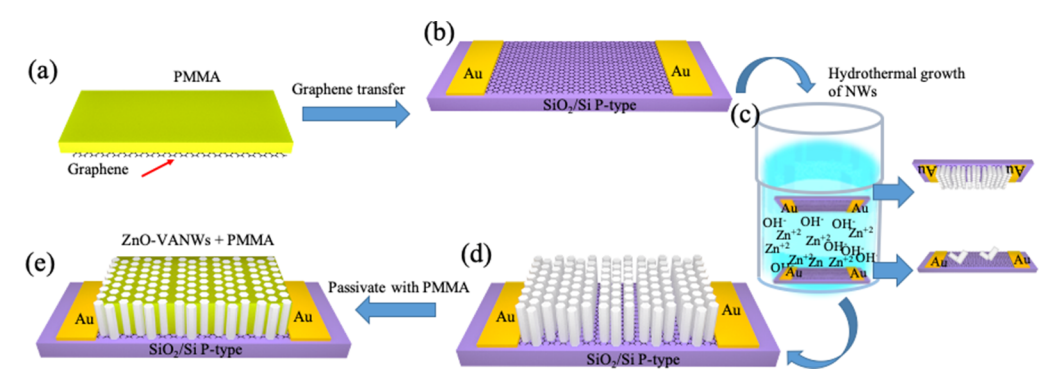


Figure 1. Schematic description of the ZnO-VANWs/Gr nanohybrid device fabrication process: (a) PMMA coated CVD Gr after Cu foil was dissolved in $FeCl_3$; (b) transferred Gr on a SiO_2/Si substrate with prefabricated Au/Ti electrodes; (c) seedless hydrothermal process with the $Gr/SiO_2/Si$ substrate facing down and floating on the surface of the solution; (d) ZnO-VANWs/Gr nanohybrids obtained in (c); and (e) passivation of the ZnO-VANWs/Gr with PMMA.

coupling. The piezoelectric potential induced on spin-coated P(VDF-TrFE) by external strains was effectively coupled to the GFET channels with a high strain sensitivity of 0.008%. Yogeswaran et al. reported a piezoelectric GFET for tactile sensing²⁸ using a polycrystalline PZT film to transduce the piezoelectric field to modulate the GFET channel conductance. At a low operating bias of 0.1 V, this sensor illustrates a sensitivity of $4.55 \times 10^{-3} \text{ kPa}^{-1}$ with a dynamic response time of a few seconds in the pressure range 23.54-94.18 kPa. Quang et al. achieved piezoelectric gating of monolayer CVD Gr from the deformation of hydrothermally grown vertically aligned ZnO vertical aligned nanowires (ZnO-VANWs) on top of a polycrystalline ZnO seed layer (ZnO-SL) coated on Gr. A sensitivity of $2.5 \times 10^{-3} \text{ kPa}^{-1}$ (64–160 kPa) and response time of 0.85 s were obtained.²⁹ It should be noted that an optimal piezoelectric gating effect can be realized when the ZnO-VANWs/Gr interface is pristine. The polycrystalline ZnO-SL is defective and hence detrimental to the ZnO-VANWs/ZnO-SL/Gr device performance due to the charge trapping by defects in the ZnO-SL that has been found to lead to slow response in ZnO-VANWs/Gr ultraviolet detectors.³⁰

Motivated by the challenges, this work explores the hydrothermal growth of (0001)-oriented crystalline ZnO-VANWs on CVD Gr using a facile seedless solution process. 30,31 ZnO is a piezoelectric semiconductor, 32 which exhibits biocompatibility 33 and radiation hardness 34,35 and more importantly can be grown into different crystalline nanostructures on Gr at low temperatures in air. 26,36 The (0001) direction is the most favorable one for the best piezoelectricity in ZnO. $^{37-39}$ The seedless ZnO-VANW growth was found critical to obtaining a low-defect ZnO-VANWs/Gr interface with minimal charge trapping, which has resulted in a remarkably improved pressure/strain sensitivity of up to $3.15\times 10^{-2}~\mathrm{kPa^{-1}}$ and a dynamic response time of $\sim\!0.10$ s compared to those in the case of ZnO-VANWs/ZnO-SL/Gr. In the following, we report our experimental results.

2. EXPERIMENTAL SECTION

2.1. Graphene Growth and Transfer. CVD Gr was grown on commercial polycrystalline copper foils (Sigma-Aldrich, USA) of 25 μ m in thickness at a temperature of 1050 °C for 30 min. Under 1 Torr of mixed gas of H₂ (7 SCCM) and CH₄ (40 sccm). 40,41 PMMA was spin-coated onto one side of the Gr samples, followed by baking on a hot plate at 80 °C for 10 min and soaking in iron chloride (FeCl₃) solution for 1 h to dissolve the Cu foil. Afterward, graphene/PMMA was cleaned thoroughly in deionized (DI) water to remove

the chemical residues on Gr before being transferred onto the $SiO_2~(300~nm)/Si$ substrates with prefabricated Au (40 nm)/Ti (10 nm) electrodes using electron-beam evaporation through a shadow mask. The details of the Gr transfer have been reported in our earlier works. 42,43 The Gr channel dimension was 0.3 mm (length) \times 3 mm (width) for the strain sensors investigated in this work. After the Gr transfer, PMMA was removed by immersing the sample in acetone for approximately 1 h, followed by soaking in isopropyl alcohol for 20 min. The samples were then annealed in a furnace at 450 °C for 15 min in flowing forming gas (H_2/Ar) to eliminate polymer residues on Gr. Although this temperature is above the eutectic temperature of $\sim\!380$ °C for Au/Si, the Au/Ti electrode remains intact considering the large Au thickness and the presence of Ti; both would prevent the eutectic Au/Si to occur. 44

2.2. Fabrication of ZnO-VANWs/Gr and ZnO Films/Gr Samples. The ZnO-VANWs were grown on Gr by floating the transferred Gr on SiO₂ (300 nm)/Si substrates in a face-down configuration in 100 mL of aqueous zinc nitrate hexahydrate solution placed in an oven at 90 °C for 4 h using a seedless ZnO-VANW growth procedure we have reported recently. 31,45 A pH value of ~10 was maintained in the zinc nitrate hexahydrate solution under constant stirring by adding a small amount of ammonium hydroxide frequently during the ZnO-VANW growth. The pH value at ~10 was found critical to obtaining dense and uniform ZnO-VANWs on Gr in the seedless growth.⁴⁵ After the ZnO-VANW growth was completed, the sample was cleaned with DI water, followed by nitrogen gas drying. A small droplet of PMMA (3% in chloroform) was cast on the ZnO-VANWs/Gr channel and allowed to dry overnight in ambient conditions for the mechanical stability of the ZnO-VANWs/Gr samples. For a comparison, polycrystalline ZnO film/Gr samples were also fabricated. Specifically, a 0.3 M Zn(Ac)2·2H2O precursor with equivalent molar quantity of ethanolamine was dissolved in 2methoxyethanol with a concentration of 0.3 wt % to make a sol gel solution by sonication. The precursor was then deposited on the Gr/ SiO₂ (300 nm)/Si substrates using spin-coating at 3000 rpm for 1 min, followed by curing at 180 °C for 10 min on a hot plate. This process was repeated 10 times to form a uniform ZnO precursor film with a thickness of ~100 nm. Finally, the precursor films were annealed at 350 °C in air for 60 min to form polycrystalline ZnO films. More details of the ZnO film growth were reported in our earlier works.

2.3. Characterization of ZnO-VANWs/Gr and ZnO Film/Gr Samples. Sample morphologies were characterized using optical microscopy and scanning electron microscopy (SEM) using Nikon Eclipse LV 150 and JEOL JSM-6380 SEM systems, respectively. Transmission electron microscopy (TEM) and high-resolution TEM (HRTEM) were employed to characterize the crystallinity of ZnO-VANWs using an FEI Tecnai F20XT system. In addition, Raman spectroscopy (WiTec alpha300) with a laser excitation wavelength of 488 nm was applied to characterize both Gr and ZnO-VANWs. Electrical connections to the Au/Ti electrodes of the ZnO-VANWs/

Gr and ZnO film/Gr strain sensors were completed using annealed Pt wires of 50 μ m in diameter for electric transport measurements. The current—voltage (I–V) characteristics and dynamic responses of the ZnO-VANWs/Gr and ZnO film/Gr sensors were measured using a CHI660D electrochemical workstation in response to the applied pressure/strain. Two approaches were employed to apply the strain to the sensors: one through application of gas pressures in a vacuum chamber and the other via application of mechanical force using a spring-loaded apparatus.

3. RESULTS AND DISCUSSION

Figure 1 depicts schematically the process developed in this work for the fabrication of the ZnO-VANWs/Gr nanohybrid strain sensors including CVD Gr transfer on SiO₂/Si substrates with prefabricated Au/Ti electrodes (Figure 1a,b), ZnO-VANW growth on Gr in the seedless hydrothermal process with the Gr/SiO₂/Si substrate floating on the surface of the solution in the face-down configuration (Figure 1c,d), and the stabilization of the ZnO-VANWs/Gr/SiO₂/Si substrates by casting PMMA on the ZnO-VANWs/Gr channel (Figure 1e). It has been found that the difference in the growth configurations, such as face-up and face-down configurations, affects the ZnO nucleation, density, and morphology dramatically. In particular, the accumulation of residues on Gr can be minimized in the face-down configuration (as opposed to the face-up one, for example),³¹ which is critical to facilitating high-density nucleation of the ZnO-VANWs on Gr. The face-down configuration leads to a much cleaner ZnO-VANW/Gr nanohybrid interface that is important to the performance of the nanohybrid devices. In contrast, only sparse ZnO nanowires without vertical alignment were obtained on Gr/substrate in the face-up configuration due to the chemical residues aggregated on Gr. 31 Unlike the processes that employ a ZnO-SL on Gr to promote the nucleation of the ZnO NWs, ZnO nucleation occurs directly on Gr in the seedless process. This leads to a cleaner ZnO-VANW/Gr interface that is important to the performance of the nanohybrid devices by removing charge traps formed in the defective ZnO-SL. 31,45 It should also be noted that the PMMA cast on ZnO-VANWs/Gr not only enhances the mechanical strength of the nanohybrid sensors but also passivates the surface of ZnO to prevent surface degradation in ambient conditions. It should be pointed out that the seedless process shown in Figure 1 is low-cost and scalable for the fabrication of the ZnO-VANWs/Gr nanohybrids.

Figure 2a depicts the optical images of Gr before (left) and after (right) the growth of the ZnO-VANWs. The negligible color contrast on Gr suggests that the Gr surface is clean, which is important to the dense and uniform nucleation of the ZnO-VANWs on Gr, as confirmed in the right image. Figure 2b,c shows the SEM images of the ZnO-VANWs taken at 60 and 85° tilt angles, respectively, with respect to the electron beam of the SEM. Densely packed and uniform ZnO-VANWs obtained in the seedless hydrothermal growth process can be clearly seen. The average diameter and length of the ZnO nanowires are 455 \pm 98 nm and 7.0 \pm 1.6 μ m, respectively. Figure 2d depicts a zoom-in top-view SEM image of the ZnO-VANWs. A hexagonal cross section of the ZnO nanowires can be clearly seen, indicating the axial direction of the crystalline ZnO-VANWs along the (0001) of the wurtzite ZnO crystal structure. Considering that the (0001) direction is energetically preferred, the formation of (0001)-oriented ZnO-VANWs on Gr can be described as the stacking of a number of alternate planes of ZnO with tetrahedrally coordinated O²⁻

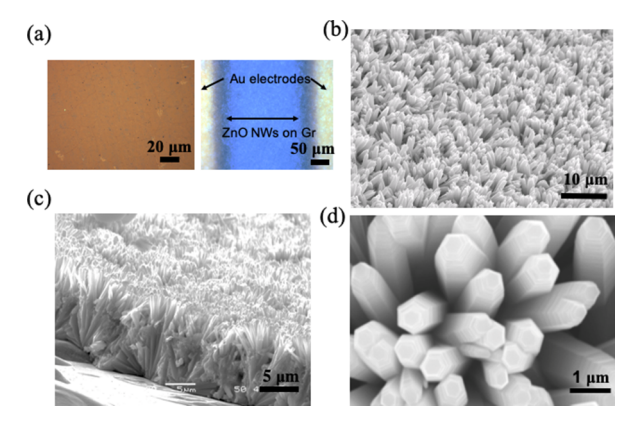


Figure 2. (a) Optical images of a pristine Gr (left) and a ZnO-VANWs/Gr (right). (b, c) SEM images taken at tilted angles of 60 and 85° with respect to the electron-beam, respectively. (d) Top-view SEM image of the ZnO-VANWs.

and Zn^{2+} ions along the (0001) axis after the initial nucleation of ZnO on Gr. 46

Figure 3a compares the Raman spectra of graphene before (black) and after (red) the ZnO-VANW growth. The

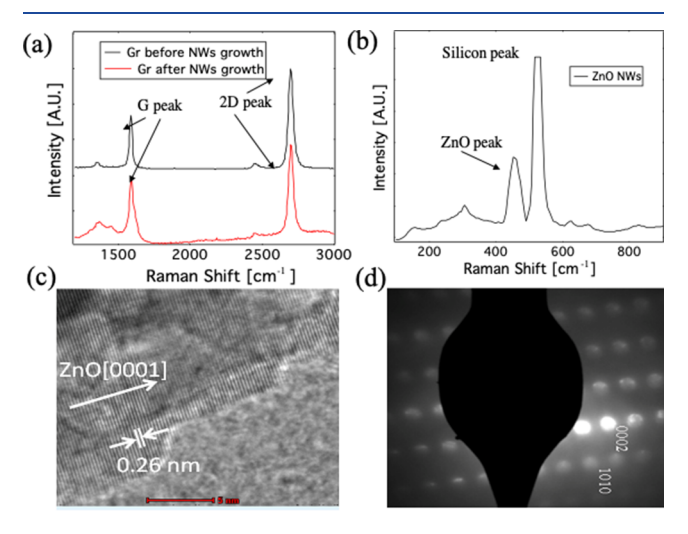


Figure 3. (a) Raman spectra of the Gr before (black) and after (red) the ZnO-VANW growth. (b) Raman spectrum taken on a ZnO-VANWs/Gr sample at low wavenumbers. (c) HRTEM image of a representative ZnO nanowire showing ZnO (0001) fringes perpendicular to the nanowire axis, separated by 0.26 nm, indicating the crystalline ZnO growth along the ZnO (0001) direction. (d) SAED pattern taken on the ZnO nanowire in (c).

characteristic Raman peaks of Gr, namely, the G peak at $\sim\!1590~{\rm cm}^{-1}$ and 2D peak at $\sim\!2715~{\rm cm}^{-1}$ can be observed on both spectra. The G peak corresponds to the ${\rm E_g}^2$ phonon at the Brillouin zone center, and the 2D peak is related to the second-order harmonic of the D peak corresponding to the ${\rm A_{1g}}$ breathing mode. The intensity ratio of 2D to G peaks (I $_{\rm 2D}/{\rm I_G}$) is around $\sim\!2$, and the full width at half-maximum (FWHM) peak is at $\sim\!34~{\rm cm}^{-1}$ before the ZnO-VANW growth, indicating that the CVD Gr is a monolayer. The D band at $\sim\!1354~{\rm cm}^{-1}$ arising from defects in Gr is negligible. In fact, the ratio of D to G band (I $_{\rm D}/{\rm I_G}$) is as low as $\sim\!0.1$. The high I $_{\rm 2D}/{\rm I_G}$ ratio and very low D peak are indicative of high-quality monolayer CVD Gr. It is particularly worth pointing out that the quality of Gr was preserved in the seedless

hydrothermal process for the growth of the ZnO-VANWs, which is essential for the optimum performance of the ZnO-VANWs/Gr nanohybrid devices. 49 In Figure 3b, the major Raman peak at ~440 cm⁻¹ is attributed to the E₂ energy mode of ZnO while the minor Raman peak at ~330 cm⁻¹ is secondorder scattering from phase boundaries of ZnO, demonstrating the formation of crystalline ZnO-VANWs on Gr during the hydrothermal growth. 50 The FWHM of this Raman signature peak for ZnO-VANWs is around 27 cm⁻¹, which is slightly higher than that for the single crystal bulk ZnO (\sim 12 cm⁻¹)^{S1} and is most probably associated with structural defects on the ZnO-VANWs grown in the hydrothermal process at low temperatures. This is a trade-off for the benefit in the direct growth of crystalline ZnO nanowires on graphene, which requires processing compatibility to maintain the quality of graphene. Figure 3c,d shows an HRTEM image of a representative ZnO nanowire removed from the ZnO-VANWs and the corresponding selected area electron diffraction (SAED) pattern taken on it, respectively. The HRTEM and SAED confirm that the ZnO nanowires are single crystals with the growth direction along the ZnO (0001) and a lattice spacing of 0.26 nm as anticipated. In fact, the ZnO (0001) is the preferred orientation for high-performance piezoelectric strain sensors based on ZnO-VANWs.^{37,3}

Figure 4a depicts the images of the vacuum chamber used for applying gas pressure with the inset showing the sample

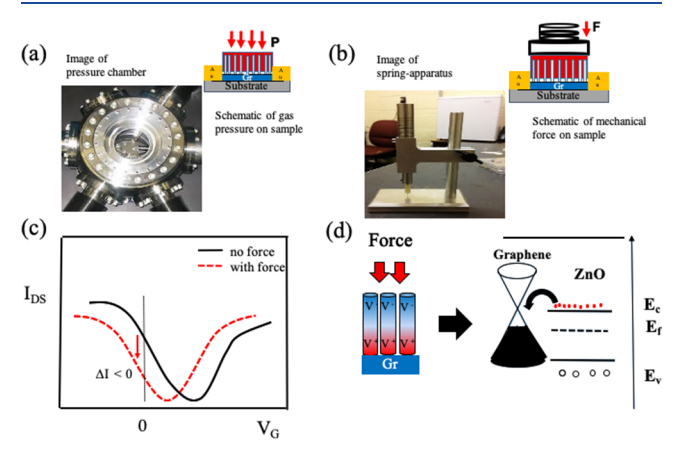


Figure 4. (a) Image of gas pressure (in a vacuum chamber) with the inset showing the schematic of sample inside the chamber where gas passed to the sample to deform the nanowires. (b) Images of compressive force (a spring-loaded apparatus) for mechanical deformation of the strain sensors with the inset showing the schematic of the apparatus. (c) Schematic of current—voltage characteristic curve of Gr showing the shift of the curve as a consequence of piezoelectric gating transduced by the ZnO-VANWs upon mechanical deformation. (d) Band edge diagram at the ZnO-VANW/Gr interface in response to the piezoelectric effect of the ZnO-VANWs under mechanical deformation.

under the gas pressure. Various nitrogen (N_2) pressures in the range of 1.1×10^{-6} –420 Torr were applied to deform ZnO-VANWs. In contrast, mechanical forces were applied using a spring-loaded piston (Figure 4b) with a spring constant of 1.23 N/mm and the applied forces were estimated based on Hook's law $(F = -k\Delta x)$, where k and Δx are the spring constant and displacement, respectively. The inset of Figure 4b illustrates schematically the sample under the applied force using the spring-loaded apparatus. In this work, the forces applied to the ZnO-VANWs/Gr nanohybrid sensors were varied in the range

of 0-0.56 N. The two approaches shown in Figure 4a,b provide complementary capabilities in the characterization of the ZnO-VANWs/Gr nanohybrid strain sensors. The former offers a wider range of mechanical deformation while the latter can be used to detect the dynamic response of the sensor to applied force pulses. In fact, the force range of 0.14-0.56 N from the spring-loaded apparatus corresponds to the pressure range of 105-420 Torr. Figure 4c explains the sensing mechanism via detecting the conductance change on the Gr channel ($\Delta \sigma = \sigma - \sigma_0$) between the conductivity with (σ) and without (σ_0) an applied pressure/force. The source-drain current versus gate voltage curve (I_{DS} vs V_G) of the Gr channel under no strain (black) is representative, as shown in our previous studies of graphene field effect transistors. 42,43,52 The Dirac point $(V_{\rm Dirac})$ located at the minimum of the $I_{\rm DS} - V_{\rm G}$ curve for the CVD Gr channel is typically at a positive V_G due to the p-type doping. This means that the conductivity of the Gr channel will be on the left branch (or hole branch) of the $I_{\rm DS} - V_{\rm G}$ curve at $V_{\rm G} = 0$, as shown by the dashed line in Figure 4c. When a piezoelectric $V_{\rm G}$ is generated by the charges accumulated at the ZnO-VANWs/Gr interface as a consequence of the mechanical deformation on the ZnO-VANWs, this piezoelectric V_G will shift the Dirac point either to the right (tensile strain) or to the left (compressive strain, which is the case in this work, as shown by the red curve in Figure 4c), depending on the polarity of the piezoelectric potential across the ZnO-VANWs. 29,53 The strain response is proportional to the $\Delta\sigma$ (illustrated by the red arrow) and the strain sensitivity is defined as the slope of the $\Delta\sigma/\sigma_0$ versus pressure/force curve. The left side of schematic in Figure 4d depicts schematically the piezoelectric charges at the two ends of ZnO-VANWs under compressive strain. The charges at the ZnO-VANW/Gr interface will cause piezoelectric gating on Gr and hence shift the source-drain current versus gate voltage curve illustrated in Figure 4c.⁵⁴ Quantitatively, this piezoelectric gate voltage applied to the Gr channel at the ZnO-VANWs/Gr interface is proportional to the surface charge density at the interface or deformation of the ZnO-VANWs, changing the Fermi level of Gr or the position of Dirac point $(V_{\rm Dirac})$ at the minimum of the I-V curve, as shown in the energy band diagram on the right side of Figure 4d. 55

Figure 5a depicts the plots of the $\Delta \sigma / \sigma_0$ versus pressure of the ZnO-VANWs/Gr (red) and ZnO film/Gr (black) devices taken inside the vacuum chamber. Both devices have a similar trend of monotonic increasing $\Delta \sigma / \sigma_0$ with increasing pressure. However, higher strain sensitivity, defined as the slope of the $\Delta \sigma / \sigma_0$ versus pressure curve, decreases monotonically with the increasing pressure. In fact, a much higher strain sensitivity can be observed in the lower pressure range up to around a few Torr in both types of devices, followed by much reduced sensitivity, as reported previously.¹⁷ The inset of Figure 5a compares the performance of ZnO-VANWs and ZnO film strain sensors at a low-pressure range of 1.1×10^{-6} to 11 Torr. Quantitatively, the ZnO-VANWs/Gr device shows a strain sensitivity of $3.15 \times 10^{-2} \text{ kPa}^{-1}$ in the lower pressure range, which decreases to $1.5 \times 10^{-3} \text{ kPa}^{-1}$ at higher pressures up to 420 Torr. Similarly, a higher sensitivity of $1.27 \times 10^{-2} \text{ kPa}^{-1}$ is observed in the ZnO film/Gr device in the lower pressure range up to ~11 Torr, which is reduced to $2.25 \times 10^{-4} \text{ kPa}^{-1}$ in the higher pressure range. Therefore, the lower the strain, the higher the strain sensitivity in both cases. However, the lower pressure sensitivity of the ZnO-VANWs/Gr devices is about 2.5 times higher than its ZnO film/Gr counterpart's in

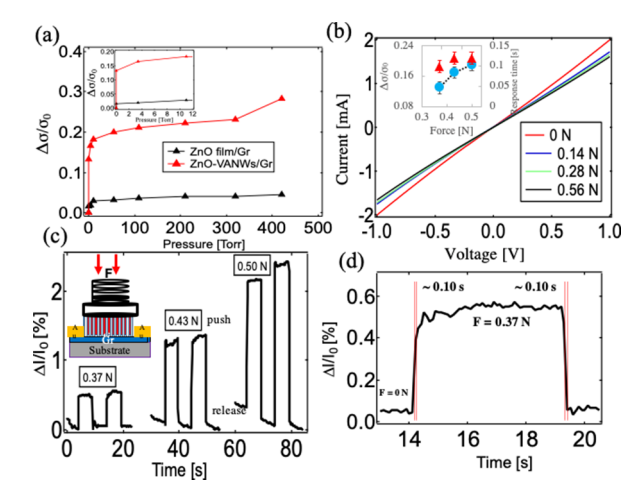


Figure 5. Characterization of the ZnO-VANWs/Gr and ZnO film/Gr strain sensors: (a) $\Delta\sigma/\sigma_0$ as a function of gas pressure measured on ZnO-VANWs/Gr (red) and ZnO film/Gr (black) devices. (b) I-V characteristic curves taken on the ZnO-VANWs/Gr device at different forces applied using the spring apparatus where the inset showing the sensitivity and response time as a function of forces. (c) Dynamic strain response at different forces of 0.37, 0.43, and 0.50 N with the inset showing schematic of the spring apparatus. (d) Zoom-in views of the rise and fall of the strain response with the corresponding response times illustrated.

the same pressure range. At higher pressures, the enhancement factor increases to 6.7. The higher sensitivity observed on the ZnO-VANWs/Gr sensors illustrates the benefits of the alignment of the (0001)-oriented ZnO-VANWs for the optimal piezoelectric gating. $^{37-39}$ Figure 5b compares the source-drain I-V curves taken at different forces of 0, 0.14, 0.28, and 0.56 N using the spring system. The slopes of the linear I-V curves represent the conductance σ values of the device at the applied forces. The lower-left inset of Figure 5b shows an approximately linear $\Delta \sigma / \sigma_0$ versus force trend in the range of applied force of 0-0.56 N and the slope of this curve is used to estimate the strain sensitivity. For the ZnO-VANWs/ Gr devices, the strain sensitivity is around $2.72 \times 10^{-3} \text{ kPa}^{-1}$ which is comparable to the sensitivity of 1.5 \times 10⁻³ kPa⁻¹ measured using the gas pressure method in the higher pressure range. This is anticipated since the finite force range of 0.14-0.56 N from the spring-loaded apparatus corresponds to the pressure range of 105-420 Torr. The response times (the same for rise and fall) at 0.37, 0.43, and 0.50 N are plotted as a function of forces in the upper-right inset of Figure 5b. It can

be clearly seen that the response time remains almost constant with small error bars at different forces. The fast and symmetric strain response indicates that the charge trapping at the ZnO-VANWs/Gr is negligible.

The dynamic responses were taken with respect to pulses of forces of 0.37, 0.43, and 0.50 N, and the result is exhibited in Figure 5c. The inset in Figure 5c shows a schematic of a spring apparatus, which was used to directly apply periodic force to obtain the dynamic response, as seen in Figure 5c. It is observed that the amplitude of the response $(\Delta I/I_0 = \Delta \sigma/\sigma_0)$ is approximately linearly dependent on the applied forces. Quantitatively, the $\Delta I/I_0$ is about 0.50% under the 0.37 N force pulses and increased to almost 2.25% at an increased force of 0.50 N (at a bias voltage of 1 V). The amplitude of the dynamic $\Delta I/I_0$ is considerably smaller than the static counterpart's at the same applied force. While the mechanism underlying this requires further investigation, we hypothesize that the presence of PMMA may hinder the complete transduction of the applied force in a short period. Response time is an important specification of the device performance and is defined by the time during which the response rises from 10 to 90% (t_{rise}) and drops from 90 to 10% (t_{fall}) of the response pulse amplitude. Sh As shown in Figure 5d, the t_{rise} and $t_{\rm fall}$ are both ~0.10 s for the ZnO-VANWs/Gr nanohybrid strain sensor, which is significantly shorter by 8 times than the ZnO-VANWs/ZnO-SL/Gr (rise/fall response times of ~0.80/ 0.85 s).²⁹ Considering a much faster piezoelectric response in single crystals as small as hundreds of microseconds, there is a room for further improvement of the ZnO-VANWs/Gr nanohybrid strain sensors by reducing the defects in ZnO-VANWs and at the ZnO-VANWs/Gr interface. In a comparative study of the two types of the ZnO-VANWs/Gr photodetectors, one grown with a polycrystalline ZnO-SL while the other in the same seedless process as that used in this work, a much slower and asymmetric (longer falling time) photoresponse was observed in the former as compared to that in the latter.³⁰ This means that the seedless growth process yields a much less defective ZnO-VANWs/Gr interface. The faster and symmetric rise/fall response times observed in the ZnO-VANWs/Gr strain sensors therefore confirm the benefit of the removal of the ZnO-SL in our seedless growth of ZnO-VANWs on Gr to achieve a much less defective ZnO-VANWs/ Gr interface required for high-performance strain sensors, photodetectors, and other devices.³⁰

In order to evaluate the contribution of the PMMA supporting layer around the ZnO-VANWs to the strain

Table 1. Performance Comparison of ZnO Nanostructure/Gr Pressure/Strain Sensor^a

type	device	method	sensitivity $\left(\frac{\Delta \sigma \Big _{\sigma_0}}{\Delta p}\right)$	range	RT	reference
PE	ZnO-VANWs/Gr	gas pressure	$3.15 \times 10^{-2} \text{ kPa}^{-1}$	$1.1 \times 10^{-6} - 11 \text{ Torr}$		this work
			$1.5 \times 10^{-3} \text{ kPa}^{-1}$	11-420 Torr		
		mechanical	$2.72 \times 10^{-3} \text{ kPa}^{-1}$	0-420 Torr	0.1 s	
PE	ZnO film/Gr	gas pressure	$2.0 \times 10^{-3} \text{ kPa}^{-1}$	1.9×10^{-6} –420 Torr		this work
			$2.25 \times 10^{-4} \text{ kPa}^{-1}$	11-400 Torr		
PE	ZnO-VANWs/ZnO-SL/Gr	gas pressure	$1.27 \times 10^{-2} \text{ kPa}^{-1}$	0-1200 Torr	0.8-0.85 s	29
PR	ZnO-VANWs/ZnO-SL/CNT/rGO	mechanical	$\Delta I/I_0 \approx 33\%$	0-6.2%	few seconds	57
PE	ZnO film/Au	mechanical	$\Delta I/I_0 \approx 20\%$	0-0.10%	few seconds	58
PE	Ag/PZT/Au	mechanical	$4.55 \times 10^{-3} \text{ kPa}^{-1}$	0-705 Torr	few seconds	28
PR	PbTiO ₃ NWs/Gr	mechanical	$9.4 \times 10^{-3} \text{ kPa}^{-1}$	0-10 Torr	5-7 ms	13

^aPR, piezoresistive; PE, piezoelectric; RT, response time.

sensitivity, PMMA/Gr reference samples were also tested with respect to the applied deformation. Figure S1a (Supporting Information) depicts an optical image of three PMMA/Gr strain sensors made on a silicon substrate with four Au/Ti electrodes. The dynamic strain response was measured on this sample at 0.7, 1.0, and 1.5 N compressive forces by the spring loaded piston (see Experimental Section in the manuscript), and the result is shown in Figure S1b. For the convenience of comparison with Figure 5c, a similar vertical scale was selected for Figure S1b. While a small strain response seemed to be visible in the PMMA/Gr sample, its magnitude is only 0.04%, which is more than two orders of magnitude smaller than the strain response of the ZnO-VANWs/Gr sample at the same applied force of 0.7 N shown in Figure 5c. Furthermore, the "strain response" of the PMMA/Gr sample does not seem to increase with the increasing applied force up to 1.5 N, casting a serious doubt whether the observed small strain response is simply caused by contact charge under mechanical deformation. This result has therefore confirmed that the piezoelectric effect on the ZnO-VANWs/Gr strain sensors is attributed to the piezoelectric potential generated across the ZnO-VANWs, which is transduced to the piezoelectric gating on the Gr channel. This confirmation is consistent with a wide adoption of PMMA as the mechanical enforcement matrix material in nanocomposites and encapsulation materials for ZnO-VANW nanogenerators.57

Table 1 compares the performance of the ZnO-VANWs/Gr strain sensors developed in this work with a list of previously reported pressure/strain sensors. In comparison with the ZnO-VANWs/ZnO-SL/Gr with a similar structure except that it adopted a ZnO-SL, the removal of the ZnO-SL leads to almost an order of magnitude enhancement in the sensitivity and 8fold reduction in t_{rise} and t_{fall} . An additional benefit is the simplification of the sensor fabrication by eliminating the ZnO-SL growth step. Furthermore, compared to some of the other piezoresistive devices (ZnO-VANWs/ZnO-SL/CNT/rGO) having a $\Delta I/I_0$ of ~33% with a few seconds of response time, our device has similar sensitivity with at least an order of magnitude better response time. The high performance of the ZnO-VANWs/Gr strain sensors may be attributed to the combined effects of the different strain sensing physics of highly sensitive piezoelectric gating on the Gr channel conductance and optimization of the device structure by vertical alignment of the ZnO nanowires in the most preferable (0001) orientation for the piezoelectric effect, together with removal of the ZnO-SL for a much less defective ZnO/Gr interface. Defects in ZnO-SL are typically responsible for the charge trapping, which is consistent with the poor crystallinity observed on the ZnO-SL, which are critical for the performance of the ZnO-VANWs/Gr optoelectronic and piezoelectric devices.³⁰ It should be mentioned that the ZnO-VANWs/Gr nanohybrid strain sensors in the strain range reported in this work have good durability with respect to repeated measurements.

4. CONCLUSIONS

In this paper, a ZnO-VANWs/Gr nanohybrid strain sensor was obtained using a seedless solution growth process for ZnO-VANWs to form on CVD Gr floating face-down in the mixed solution of zinc nitrate hexahydrate and ammonia hydroxide. A clean Gr surface and the pH value of $\sim \! 10$ were both found critical to the achievement of dense (0001)-oriented crystalline ZnO-VANWs on Gr. The (0001)-oriented ZnO-VANWs can

provide the optimal transduction of mechanical deformation to piezoelectric gating on Gr, resulting in high strain sensitivity. Two complementary schemes were deployed to generate mechanical deformation on the ZnO-VANWs/Gr nanohybrid strain sensors including gas pressure in the range of 1.1 X 10^{-6} – 420 Torr and compressive forces of 0.14 – 0.56 N (105 – 420 Torr) using a spring-loaded apparatus. Using the former, high strain sensitivity up to $3.15 \times 10^{-2} \text{ kPa}^{-1}$ was obtained in the low pressure range of 1.1×10^{-6} –11 Torr. At higher pressures, a sensitivity of $2.72 \times 10^{-3} \text{ kPa}^{-1}$ was obtained under 1.0 V bias voltage. The values are 3 and 7 times, respectively, better than their ZnO film/Gr counterparts' in the same pressure ranges. The higher sensitivity of the ZnO-VANWs/Gr nanohybrid strain sensors can be ascribed to the (0001)-oriented crystalline ZnO-VANWs with the optimal transduction of the mechanical deformation to piezoelectric gating on Gr. In contrast, the piezoelectric effects from many different grains of random orientations may be cancelled over a large sensor scale of hundreds of micrometers. In addition, the ZnO-VANWs/Gr nanohybrid strain sensors have a fast and reproducible dynamic strain response with both rise and fall strain response time of 0.10 s. In comparison with the similar device of ZnO-VANWs/ZnO-SL/Gr, the sensitivity and response time of the ZnO-VANWs/Gr nanohybrid strain sensors obtained in the seedless hydrothermal process are almost an order of magnitude better, which reveals the importance of a clean (less defective) interface in the latter by removing the polycrystalline ZnO-SL. It should be realized that higher performance may be achieved on ZnO-VANWs/Gr nanohybrid strain sensors by further reducing the growth defects in ZnO-VANWs for optimized piezoelectric gating effect on the Gr channel. Finally, the low-cost, seedless hydrothermal process developed for the fabrication of the ZnO-VANWs/Gr nanohybrids can be readily scaled up for practical applications.

ASSOCIATED CONTENT

Supporting Information

The Supporting Information is available free of charge at https://pubs.acs.org/doi/10.1021/acsanm.0c01150.

Photograph of three PMMA/Gr strain sensors on the SiO_2/Si substrate with prefabricated Au/Ti electrodes and dynamic response of the sample at various forces of 0.7, 1.0, and 1.5 N (PDF)

AUTHOR INFORMATION

Corresponding Authors

Mohan Panth — Department of Physics and Astronomy,
University of Kansas, Lawrence, Kansas 66045, United States;

o orcid.org/0000-0002-4895-3527; Email: panthm@ku.edu

Judy Wu — Department of Physics and Astronomy, University of
Kansas, Lawrence, Kansas 66045, United States; Email: jwu@ku.edu

Authors

Brent Cook — Department of Physics and Astronomy, University of Kansas, Lawrence, Kansas 66045, United States;
ocid.org/0000-0001-9288-7267

Young Zhang — Department of Physics and Astronomy, University of Kansas, Lawrence, Kansas 66045, United States Dan Ewing — Department of Energy's Kansas City National Security Campus, Kansas City, Missouri 64147, United States

- Ashely Tramble Department of Energy's Kansas City National Security Campus, Kansas City, Missouri 64147, United States
- Amy Wilson Department of Energy's Kansas City National Security Campus, Kansas City, Missouri 64147, United States

Complete contact information is available at: https://pubs.acs.org/10.1021/acsanm.0c01150

Notes

The authors declare no competing financial interest.

ACKNOWLEDGMENTS

This research was supported by Plant Directed Research and Development funds from the Department of Energy's National Security Campus, operated and managed by Honeywell Federal Manufacturing and Technologies, LLC under Contract No. DE-NA0002839. J.W. acknowledges support in part by ARO Contract No. ARO-W911NF-16-1-0029 and NSF Contract Nos. NSF- ECCS-1809293, NSF-DMR-1909292, and NSF-DMR-1508494.

REFERENCES

- (1) Lee, M.; Chen, C. Y.; Wang, S.; Cha, S. N.; Park, Y. J.; Kim, J. M.; Chou, L. J.; Wang, Z. L. A hybrid piezoelectric structure for wearable nanogenerators. Adv. Mater. 2012, 24, 1759-1764.
- (2) Pan, C.; Dong, L.; Zhu, G.; Niu, S.; Yu, R.; Yang, Q.; Liu, Y.; Wang, Z. L. High-resolution electroluminescent imaging of pressure distribution using a piezoelectric nanowire LED array. Nat. Photonics 2013, 7, 752-758.
- (3) Peng, Y.; Que, M.; Lee, H. E.; Bao, R.; Wang, X.; Lu, J.; Yuan, Z.; Li, X.; Tao, J.; Sun, J.; Zhai, J.; Lee, K. J.; Pan, C. Achieving highresolution pressure mapping via flexible GaN/ ZnO nanowire LEDs array by piezo-phototronic effect. Nano Energy 2019, 58, 633-640.
- (4) Saudabayev, A.; Varol, H. A. Sensors for robotic hands: A survey of state of the art. IEEE Access 2015, 3, 1765-1782.
- (5) Giurgiutiu, V. Structural health monitoring: with piezoelectric wafer active sensors; Elsevier: 2007.
- (6) Bhalla, S.; Yang, Y. W.; Zhao, J.; Soh, C. K. Structural health monitoring of underground facilities-Technological issues and challenges. Tunnelling Underground Space Technol, 2005, 20, 487-
- (7) Papageorgiou, D. G.; Kinloch, I. A.; Young, R. J. Mechanical properties of graphene and graphene-based nanocomposites. Prog. Mater. Sci. 2017, 90, 75-127.
- (8) Geim, A. K.; Novoselov, K. S. The rise of graphene. In Nanoscience and Technology: A Collection of Reviews from Nature Journals, World Scientific: 2010; pp 11-19.
- (9) Alamusi; Hu, N.; Fukunaga, H.; Atobe, S.; Liu, Y.; Li, J. Piezoresistive strain sensors made from carbon nanotubes based polymer nanocomposites. Sensors 2011, 11, 10691-10723.
- (10) Yan, C.; Wang, J.; Kang, W.; Cui, M.; Wang, X.; Foo, C. Y.; Chee, K. J.; Lee, P. S. Highly stretchable piezoresistive graphenenanocellulose nanopaper for strain sensors. Adv. Mater. 2014, 26,
- (11) Sirohi, J.; Chopra, I. Fundamental understanding of piezoelectric strain sensors. J. Intell. Mater. Syst. Struct. 2016, 11, 246-257.
- (12) Zhang, Y.; Liu, Y.; Wang, Z. L. Fundamental theory of piezotronics. Adv. Mater. 2011, 23, 3004-3013.
- (13) Chen, Z.; Wang, Z.; Li, X.; Lin, Y.; Luo, N.; Long, M.; Zhao, N.; Xu, J.-B. Flexible piezoelectric-induced pressure sensors for static measurements based on nanowires/graphene heterostructures. ACS Nano 2017, 11, 4507-4513.
- (14) Kwon, J.; Seung, W.; Sharma, B. K.; Kim, S.-W.; Ahn, J.-H. A high performance PZT ribbon-based nanogenerator using graphene transparent electrodes. Energy Environ. Sci. 2012, 5, 8970-8975.

- (15) Qiu, Y.; Zhang, H.; Hu, L.; Yang, D.; Wang, L.; Wang, B.; Ji, J.; Liu, G.; Liu, X.; Lin, J.; Li, F.; Han, S. Flexible piezoelectric nanogenerators based on ZnO nanorods grown on common paper substrates. Nanoscale 2012, 4, 6568-6573.
- (16) Karan, S. K.; Bera, R.; Paria, S.; Das, A. K.; Maiti, S.; Maitra, A.; Khatua, B. B. An approach to design highly durable piezoelectric nanogenerator based on self-poled PVDF/AlO-rGO flexible nanocomposite with high power density and energy conversion efficiency. Adv. Energy Mater. 2016, 6, 1601016.
- (17) Chen, Y.-S.; Hsieh, G.-W.; Chen, S.-P.; Tseng, P.-Y.; Wang, C.-W. Zinc oxide nanowire-poly (methyl methacrylate) dielectric layers for polymer capacitive pressure sensors. ACS Appl. Mater. Interfaces 2014, 7, 45-50.
- (18) Xiao, X.; Yuan, L.; Zhong, J.; Ding, T.; Liu, Y.; Cai, Z.; Rong, Y.; Han, H.; Zhou, J.; Wang, Z. L. High-strain sensors based on ZnO nanowire/polystyrene hybridized flexible films. Adv. Mater. 2011, 23, 5440-5444.
- (19) Novoselov, K. S.; Geim, A. K.; Morozov, S. V.; Jiang, D.; Zhang, Y.; Dubonos, S. V.; Grigorieva, I. V.; Firsov, A. A. Electric field effect in atomically thin carbon films. Science 2004, 306, 666-669.
- (20) Zhao, J.; He, C.; Yang, R.; Shi, Z.; Cheng, M.; Yang, W.; Xie, G.; Wang, D.; Shi, D.; Zhang, G. Ultra-sensitive strain sensors based on piezoresistive nanographene films. Appl. Phys. Lett. 2012, 101, No. 063112.
- (21) Ponnamma, D.; Guo, Q.; Krupa, I.; Al-Maadeed, M. A. S. A.; Varughese, K. T.; Thomas, S.; Sadasivuni, K. K. Graphene and graphitic derivative filled polymer composites as potential sensors. Phys. Chem. Chem. Phys. 2015, 17, 3954-3981.
- (22) Tang, Y.; Zhao, Z.; Hu, H.; Liu, Y.; Wang, X.; Zhou, S.; Qiu, J. Highly Stretchable and Ultrasensitive Strain Sensor Based on Reduced Graphene Oxide Microtubes-Elastomer Composite. ACS Appl. Mater. Interfaces 2015, 7, 27432-27439.
- (23) Carter, S.; Ned, A.; Chivers, J.; Bemis, A. Selecting piezoresistive vs. piezoelectric pressure transducers; Kulite Semiconductor Products, Inc 2016.
- (24) Kon, S.; Oldham, K.; Horowitz, R. Piezoresistive and piezoelectric MEMS strain sensors for vibration detection, In Sensors and Smart Structures Technologies for Civil, Mechanical, and Aerospace Systems 2007, International Society for Optics and Photonics: 2007; p
- (25) Wang, Z. L.; Wu, W. Piezotronics and piezo-phototronics: fundamentals and applications. Nat. Sci. Rev. 2014, 1, 62-90.
- (26) Kumar, B.; Lee, K. Y.; Park, H.-K.; Chae, S. J.; Lee, Y. H.; Kim, S.-W. Controlled growth of semiconducting nanowire, nanowall, and hybrid nanostructures on graphene for piezoelectric nanogenerators. ACS Nano 2011, 5, 4197-4204.
- (27) Sun, Q.; Seung, W.; Kim, B. J.; Seo, S.; Kim, S.-W.; Cho, J. H. Active Matrix Electronic Skin Strain Sensor Based on Piezopotential-Powered Graphene Transistors. Adv. Mater. 2015, 27, 3411-3417.
- (28) Yogeswaran, N.; Navaraj, W. T.; Gupta, S.; Liu, F.; Vinciguerra, V.; Lorenzelli, L.; Dahiya, R. Piezoelectric graphene field effect transistor pressure sensors for tactile sensing. Appl. Phys. Lett. 2018, 113, No. 014102.
- (29) Quang Dang, V.; Kim, D.-I.; Thai Duy, L.; Kim, B.-Y.; Hwang, B.-U.; Jang, M.; Shin, K.-S.; Kim, S.-W.; Lee, N.-E. Piezoelectric coupling in a field-effect transistor with a nanohybrid channel of ZnO nanorods grown vertically on graphene. Nanoscale 2014, 6, 15144-15150.
- (30) Cook, B.; Liu, Q.; Liu, J.; Gong, M.; Ewing, D.; Casper, M.; Stramel, A.; Wu, J. Facile zinc oxide nanowire growth on graphene via a hydrothermal floating method: towards Debye length radius nanowires for ultraviolet photodetection. J. Mater. Chem. C 2017, 5, 10087-10093.
- (31) Liu, J.; Lu, R.; Xu, G.; Wu, J.; Thapa, P.; Moore, D. Development of a Seedless Floating Growth Process in Solution for Synthesis of Crystalline ZnO Micro/Nanowire Arrays on Graphene: Towards High-Performance Nanohybrid Ultraviolet Photodetectors. Adv. Funct. Mater. 2013, 23, 4941-4948.

- (32) Jagadish, C.; Pearton, S. J. Zinc oxide bulk, thin films and nanostructures: processing, properties, and applications; Elsevier: 2011.
- (33) Gopikrishnan, R.; Zhang, K.; Ravichandran, P.; Baluchamy, S.; Ramesh, V.; Biradar, S.; Ramesh, P.; Pradhan, J.; Hall, J. C.; Pradhan, A. K.; Ramesh, G. T. Synthesis, characterization and biocompatibility studies of zinc oxide (ZnO) nanorods for biomedical application. *Nano-Micro Lett.* **2010**, *2*, 31–36.
- (34) Zhang, Y.; Ram, M. K.; Stefanakos, E. K.; Goswami, D. Y. Synthesis, Characterization, and Applications of ZnO Nanowires. *J. Nanomater.* **2012**, *2012*, 1–22.
- (35) Anderson, J.; van de Walle, C. G. Fundamentals of zinc oxide as a semiconductor. *Rep. Prog. Phys.* **2009**, *72*, 126501.
- (36) Djurišić, A. B.; Chen, X.; Leung, Y. H.; Ng, A. M. C. ZnO nanostructures: growth, properties and applications. *J. Mater. Chem.* **2012**, 22, 6526–6535.
- (37) Romano, G.; Mantini, G.; Carlo, A. D.; D'Amico, A.; Falconi, C.; Wang, Z. L. Piezoelectric potential in vertically aligned nanowires for high output nanogenerators. *Nanotechnology* **2011**, *22*, 465401.
- (38) Han, W.; Zhou, Y.; Zhang, Y.; Chen, C.-Y.; Lin, L.; Wang, X.; Wang, S.; Wang, Z. L. Strain-Gated Piezotronic Transistors Based on Vertical Zinc Oxide Nanowires. ACS Nano 2012, 6, 3760–3766.
- (39) Hinchet, R.; Lee, S.; Ardila, G.; Montès, L.; Mouis, M.; Wang, Z. L. Performance optimization of vertical nanowire-based piezo-electric nanogenerators. *Adv. Funct. Mater.* **2014**, *24*, 971–977.
- (40) Xu, G.; Liu, J.; Wang, Q.; Hui, R.; Chen, Z.; Maroni, V. A.; Wu, J. Plasmonic Graphene Transparent Conductors. *Adv. Mater.* **2012**, 24, OP71–OP76.
- (41) Lu, R.; Konzelmann, A.; Xu, F.; Gong, Y.; Liu, J.; Liu, Q.; Xin, M.; Hui, R.; Wu, J. Z. High sensitivity surface enhanced Raman spectroscopy of R6G on in situ fabricated Au nanoparticle/graphene plasmonic substrates. *Carbon* **2015**, *86*, 78–85.
- (42) Lu, R.; Liu, J.; Luo, H.; Chikan, V.; Wu, J. Z. Graphene/GaSe-Nanosheet Hybrid: Towards High Gain and Fast Photoresponse. *Sci. Rep.* **2016**, *6*, 19161.
- (43) Xu, G.; Lu, R.; Liu, J.; Chiu, H.-Y.; Hui, R.; Wu, J. Z. Photodetection Based on Ionic Liquid Gated Plasmonic Ag Nanoparticle/Graphene Nanohybrid Field Effect Transistors. *Adv Opt Mater* **2014**, *2*, 729–736.
- (44) Pinardi, A. L.; Leake, S. J.; Felici, R.; Robinson, I. K. Formation of an Au-Si eutectic on a clean silicon surface. *Phys. Rev. B* **2009**, *79*, No. 045416
- (45) Liu, Q.; Gong, M.; Cook, B.; Ewing, D.; Casper, M.; Stramel, A.; Wu, J. Fused Nanojunctions of Electron-Depleted ZnO Nanoparticles for Extraordinary Performance in Ultraviolet Detection. *Adv. Mater. Interfaces* **2017**, *4*, 1601064.
- (46) Hwang, J. O.; Lee, D. H.; Kim, J. Y.; Han, T. H.; Kim, B. H.; Park, M.; No, K.; Kim, S. O. Vertical ZnO nanowires/graphene hybrids for transparent and flexible field emission. *J. Mater. Chem.* **2011**, *21*, 3432–3437.
- (47) Ferrari, A. C.; Basko, D. M. Raman spectroscopy as a versatile tool for studying the properties of graphene. *Nat. Nanotechnol.* **2013**, *8*, 235–246.
- (48) Pan, G.; Li, B.; Heath, M.; Horsell, D.; Wears, M. L.; Al Taan, L.; Awan, S. Transfer-free growth of graphene on SiO2 insulator substrate from sputtered carbon and nickel films. *Carbon* **2013**, *65*, 349–358.
- (49) Ferrari, A. C. Raman spectroscopy of graphene and graphite: Disorder, electron—phonon coupling, doping and nonadiabatic effects. *Solid State Commun.* **2007**, *143*, 47–57.
- (50) Zheng, M. J.; Zhang, L. D.; Li, G. H.; Shen, W. Z. Fabrication and optical properties of large-scale uniform zinc oxide nanowire arrays by one-step electrochemical deposition technique. *Chem. Phys. Lett.* **2002**, *363*, 123–128.
- (51) Lupan, O.; Pauporté, T. Hydrothermal treatment for the marked structural and optical quality improvement of ZnO nanowire arrays deposited on lightweight flexible substrates. *J. Cryst. Growth* **2010**, 312, 2454–2458.
- (52) Gong, M.; Liu, Q.; Cook, B.; Kattel, B.; Wang, T.; Chan, W.-L.; Ewing, D.; Casper, M.; Stramel, A.; Wu, J. Z. All-printable ZnO

- quantum dots/Graphene van der Waals heterostructures for ultrasensitive detection of ultraviolet light. ACS Nano 2017, 11, 4114.
- (53) Ma, C.; Lu, R.; Hu, G.; Han, J.; Liu, M.; Li, J.; Wu, J. Detecting Electric Dipoles Interaction at the Interface of Ferroelectric and Electrolyte Using Graphene Field Effect Transistors. ACS Appl. Mater. Interfaces 2017, 9, 4244–4252.
- (54) Zhou, J.; Gu, Y.; Fei, P.; Mai, W.; Gao, Y.; Yang, R.; Bao, G.; Wang, Z. L. Flexible piezotronic strain sensor. *Nano Lett.* **2008**, *8*, 3035–3040.
- (55) Geim, A. K. Graphene: Status and Prospects. Science 2009, 324, 1530–1534.
- (56) Anand, A.; Bhatnagar, M. C. Role of vertically aligned and randomly placed zinc oxide (ZnO) nanorods in PVDF matrix: Used for energy harvesting. *Mater. Today Energy* **2019**, *13*, 293–301.
- (57) Lee, T.; Lee, W.; Kim, S. W.; Kim, J. J.; Kim, B. S. Flexible textile strain wireless sensor functionalized with hybrid carbon nanomaterials supported ZnO nanowires with controlled aspect ratio. *Adv. Funct. Mater.* **2016**, *26*, 6206–6214.
- (58) Gullapalli, H.; Vemuru, V. S. M.; Kumar, A.; Botello-Mendez, A.; Vajtai, R.; Terrones, M.; Nagarajaiah, S.; Ajayan, P. M. Flexible piezoelectric ZnO-paper nanocomposite strain sensor. *Small* **2010**, *6*, 1641–1646.